On the radiation belt location in the 23 – 24 solar cycles

Alexei V. Dmitriev[1,2]

[1]Institute of Space Science, National Central University, Jhongli, Taiwan,

[2]Skobeltsyn Institute of Nuclear Physics, Lomonosov Moscow State University, Moscow, Russia,

Corresponding author: Alexei Dmitriev (dalex@jupiter.ss.ncu.edu.tw)

Abstract

Within the last two solar cycles (from 2001 to 2018), the location of the outer radiation belt (ORB) was determined with using NOAA/Polar-orbiting Operational Environmental Satellite observations of energetic electrons with energies above 30 keV. It was found that the ORB was shifted a little (~1 degrees) in the European and North American sectors while in the Siberian sector, ORB was displaced equatorward by more than 3 degrees. The displacements corresponded qualitatively to the change of geomagnetic field predicted by the IGRF-12 model. However in the Siberian sector, the model has a tendency to underestimate the equatorward shift of ORB. The shift became prominent after 2012 that might be related to a geomagnetic jerk occurred in 2012 – 2013. The displacement of ORB to lower latitudes in the Siberian sector can contribute to an increase in the occurrence rate of mid-latitude auroras observed in the Eastern Hemisphere.

Keywords: electron radiation belt, secular geomagnetic variation, mid-latitude aurora

1. Introduction

The outer radiation belt (ORB) is populated by energetic and relativistic electrons trapped in the outer zone of the magnetosphere at drift shells above L ~ 3. The outer zone and ORB are very dynamic and exhibit variations in a wide temporal range: short-term storm-time and local time variations, 27-day solar rotation, annual and solar cycle variations (e.g. Li et al., 2001; Miyoshi and Kataoka, 2011). It was shown that the location of ORB varies with the solar cycle, namely, the maximum of ORB is mostly distant from the Earth in solar minimum (Miyoshi et al., 2004). The ORB is substantially disturbed during magnetic storms (Baker et al., 2016; Shen et al., 2017). The storm-time variation is the strongest one for both the ORB location and intensity. Enhanced geomagnetic activity results in Earthward shifting of ORB. The annual variation of ORB is a manifestation of the seasonal variation in the geomagnetic activity (Li et al., 2001).

Apparently, the intense variations mask relatively weak long-term changes related to a secular variation of the core and crustal magnetic fields. Recently, a number of authors reported significant changes in the Earth's magnetic field. The magnetic axial dipole has decreased over the past 175 years by 9% (e.g. Finlay et al., 2016). It was also shown that the north magnetic dip pole, the point where the magnetic field inclination is vertical, drifted from Canada toward Siberia with the speed rapidly increasing from 10 km/yr in 1990s to more than 50 km/yr at present (Chulliat et al., 2010; Thebault et al. 2015). From 1989 to 2002, most dramatic magnetic field changes of >50 nT/yr have been found in the Canadian Arctic and Eastern Siberia.

The effects of dipole decay and pole drift are predicted by International Geomagnetic Reference Field 12th generation (IGRF-12) model (e.g. Thebault et al. 2015). However in the Siberian sector, significant anomalies of the main geomagnetic field were found at high latitudes within the 80º-130º longitudinal range (Gvishiani et al., 2014). In this sense, independent verification of changes in the geomagnetic field at high and middle latitudes is required. Namely, the decrease of magnetic dipole should result in a global equatorward shifting of the outer magnetospheric domains such as ORB and auroral region. The drift of the north magnetic pole should cause a decrease(increase) of ORB and auroral latitudes in the Siberian(North American) sectors.

The long-term changes in the location of auroral region were reported by Smith et al. (2017). They analyzed the latitudinal location of auroral electro jet (AEJ) and revealed a prominent latitudinal displacement of the AEJ by several degrees in the years 2004 – 2014 relative to the previous solar maxima in 1970 and 1980. Namely, in the Siberian sector, AEJ shifted to lower latitudes and in the American sector, AEJ shifted to higher latitudes. The opposite shifts in different sectors cannot be explained by the solar cycle variation and, thus, it has been attributed to the core and crustal magnetic fields. On the other hand, the technique of auroral precipitations is hard to use for tracing of the long-term geomagnetic variations because of high variability in the intensity, location and extension of aurora (e.g. Cresswell-Moorcock et al., 2013; Smith et al.; 2017).

An additional support of prominent changes in the geomagnetic field can be found from a sudden increase of occurrence of aurora borealis during the years of 2015 to 2017. There were numerous reports about aurora borealis observed at middle latitudes in the North America, Europe and Russia. Table 1 lists the days when discrete aurora was detected in big Russian cities Moscow (geographic location 55°45N 37°37E), St. Petersburg (geographic location 59°57N 30°18E) and Novosibirsk (geographic location 55°01N 82°55E). It is important to note that while in the North American region, the mid-latitude discrete aurora is observed quite often, this phenomenon is rare at lower magnetic latitudes such as in the regions of Central Europe and in particular in Central Russia (MacDonald et al., 2015; Vázquez et al., 2016). The previous low-latitude aurora borealis was observed during extremely strong geomagnetic storms with minimum *Dst* < -300 nT on October - November 2003 (e.g. Shiokawa et al., 2005; Mikhalev et al., 2004; Kataoka et al., 2015).

In contrast, magnetic storms in 2015 – 2017 were not very intense, as one can see in Table 1. The strongest storm on 17 – 18 March 2015, so-called St. Patrick’s Day storm, had minimum *Dst* of -220 nT. During the St. Patrick’s Day storm, aurora borealis was observed worldwide in North America, Central Europe (e.g. “Strongest geomagnetic storm of SC24 sparks spectacular aurora display” at https://watchers.news/2015/03/18/) and in a number of cities in Central Russia and Siberia (e.g. https://www.rt.com/news/241845-aurora-borealis-central-russia/). Case et al. (2015) found that during the storm, the discrete aurora was observed at unusually low latitudes, which were much lower than those predicted by models of Roble and Ridley (1987) and Newell et al. (2010).

The aurora is produced by charged particles precipitating from the outer regions of the magnetosphere to the high-latitude atmosphere. The charged particles move along the magnetic field lines and, thus, the location of precipitation is controlled both by the location of source and by the geomagnetic field configuration. In the present study, we analyze the configuration of the outer magnetosphere by using observations of energetic electrons from ORB. At low heights, the ORB electrons are observed at middle to high latitudes adjacent to the region of auroral precipitations (Lam et al., 2010). Here we use experimental data on energetic electrons measured by several low-earth orbit (LEO) polar orbiting satellites during the time period from 1998 to 2016. The method of analysis is described in section 2. The results are presented and discussed in sections 3 and 4, respectively. Section 5 is conclusions.

2. Method

Energetic electrons in energy ranges >30 keV, >100 keV and >300 keV are measured at LEO by the Medium Energy Proton and Electron Detector (MEPED) instruments on board the NOAA/Polar-orbiting Operational Environmental Satellite (POES) satellites (Evans and Greer, 2004; Asikainen and Mursula 2013). Six POES satellites NOAA-16, NOAA-17, NOAA-18, NOAA-19, METOP-01 and METOP-02 (hereafter, P6, P7, P8, P9, P1 and P2, respectively) have Sun-synchronous orbits at altitudes of ~800-850 km in different local time sectors. Different POES satellites were operating during different years as shown in Table 2.

The outer magnetosphere and ORB are very dynamic regions, which are directly controlled by highly variable solar wind plasma streams and interplanetary magnetic field (IMF). As a result, the location of ORB and its high-latitude projection to the heights of LEO vary substantially (e.g. Dmitriev et al., 2010; Rodger et al., 2010). Namely, a strong local time variation is related to the global day-night asymmetry of the magnetosphere such that ORB is observed at higher latitudes during daytime. Variation of geomagnetic tilt angle also causes a change of the ORB latitudinal location. Interplanetary and geomagnetic disturbances result in a prominent equatorward shift of ORB.

In order to eliminate the disturbing factors, we consider so-called quiet days. Figure 1 demonstrates an example of geomagnetic conditions and measurements of the solar wind plasma and IMF acquired from Wind upstream monitor during quiet day on 23 June 2006. At that day, the solar wind velocity was slow (~310 km/s), solar wind dynamic pressure was slightly varying about ~1.6 nPa, IMF had northward orientation that resulted in very quiet geomagnetic activity (*AE* < 100 nT, *Dst* ~ 0 nT).

The list of quiet days selected in the time interval from 2001 to 2018 is presented in Table 2. The solar wind data were acquired from Wind upstream monitor. The selection of quiet days was based on the following criteria:

1. The *Dst* variation was close to 0 and *AE* index was smaller than 200 nT, i.e. the geomagnetic activity was very week.

2. The solar wind dynamic pressure *P*d varied slightly around its average values falling in the range from ~1 to 2 nPa.

3. The solar wind speed was <400 km/s and the amplitudes of negative IMF Bz were weak (<4 nT). Note that fast solar wind with the speed of V > 400 km/s initiates the Kelvin-Helmholtz instability at the magnetopause and intensification of wave activity in the outer magnetosphere that results in effective acceleration and outward transport of the ORB electrons (Engebretsone et al., 1998; Horne et al., 2007; Reeves et al., 2013).

4. The quiet days were chosen as long as possible after magnetic storms such that storm-time disturbances of ORB had time to relax. Usually, the quiet days occurred after long-lasting recovery phase of recurrent magnetic storms (Suvorova et al., 2013).

The local time variation of ORB latitudinal location was minimized by a choice of narrow LT sector around noon (from 10 to 14 LT). We chose quiet days around June solstice in order to minimize the tilt angle variations. Note that June of 2003 and 2007 was very disturbed and there were no quiet days selected for those years.

Figure 2 shows an example of NOAA/POES measurements of energetic electrons in geographic coordinates during the quiet days on 23 June 2006 and 3 June 2016. The geographic maps are composed from data retrieved over multiple orbits of the NOAA/POES satellites in the noon sector (12±2 LT). For each bin of 3° in longitudes and 0.5° in latitudes, we calculate the average flux of electrons measured by the 90° detector of the MEPED instrument. At high latitudes, the detector observes trapped electrons with pitch angles close to 90°, i.e. near the mirror points.

The limitation of ORB measurements at given local time is originated from fixed local time of POES satellites at sun synchronous orbits. As one can see in Figure 2 and Table 2, large statistics in the Northern hemisphere can be obtained from a number of POES satellites moving in 2-hour vicinity of local noon around the June solstice. ORB can be easily identified as a wide belt of intense electron fluxes at high litutudes. At middle latitudes, in longitudinal ranges from ~90°E to 180°E in the Eastern Hemisphere and from ~80°W to 180°W in the Western Hemisphere, one can also see intense electron fluxes from the inner electron belt and a slot region between the outer and inner belts. The slot region is almost vanished in the maps of subrelativistic electrons with energies >300 keV. Qualitative examination of the ORB location in Figure 2 reveals that in the Eastern Hemisphere, the outer electron belt in 2016 is located few degrees lower in latitudes than that in the year 2006. Most obvious difference can be found for the slot region, which corresponds to the low-latitude boundary of ORB.

For quantitative determination of the ORB latitudinal displacement, we analyze electron fluxes in 4° vicinities of three longitudes: 80°W (American sector), 0°E (European sector) and 100°E (Siberian sector). Figure 3 shows latitudinal profiles of >30 keV; >100 keV and >300 keV electron fluxes with pitch angles of ~90° observed by the NOAA/POES satellites around given longitudes during the quiet days in the years from 2001 to 2018. One can easily identify the maximum of ORB at high latitudes and the slot region at middle latitudes for the American and Siberian sectors. Above the Europe, the slot region is not detected at altitudes of the NOAA/POES orbit.

It should be noted that after the year 2014, the experimental data on electrons detected by POES is presented in a different format such that the energy channels of electrons are different from those presented earlier: >40 keV instead of >30 keV, >130 keV instead of >100 keV, and >290 keV instead of >300 keV. Because of that cross-calibration of the electron detectors is difficult. On the other hand, the difference in energies is not very large and, thus, it should not affect strongly the location of ORB. At least the differences are much smaller than the steps between the channels. Therefore, the complex analysis of all three electron channels allows minimization of this effect.

3. Results

In Figure 3, the ORB maxima in the American, European and Siberian sectors can be found in the ranges of latitudes from 50° to 58°, from 64° to 70° and from 62° to 74°, respectively. We determine geographic latitude of the maxima for each year with the accuracy of 0.5° to 1°. One can see that the location as well as the intensity of the maximum varies from year to year. The intensity is minimal during the solar minimum in 2009. The fluxes of >300 keV electrons (Figure 3c) were very weak such as determination of the ORB was very difficult. In addition, the ORB maximum above Siberia could not be determined in 2011 because of limited statistics.

Qualitatively, the position of ORB maximum above Siberia is more close to 70° and 65°, respectively, in 2001 - 2010 and in 2012 – 2018. Above the Europe and North America, variation of the ORB location is more random. The fluxes of >30 keV electrons in the outer region of ORB are very dynamic because of strong contribution from the auroral population. The latter produced additional maxima at latitudes above 70° and 55°, respectively, in the European-Siberian and American sectors. The additional maxima were very intense in the years 2008, 2010 and 2017 that made difficult to determine the actual location of the ORB. In those cases, we chose the maximum located at lower latitude. This choice gives a good agreement with the ORB maximum location for the >100 keV electrons and especially subrelativistic >300 keV electrons, which are practically free from the auroral contamination.

In Figure 3, one can clearly see the slot region between the outer and inner electron belts in the latitudinal ranges 45° - 50° and 45° - 50° above North America and Siberia, respectively. This structure can be well identified and numerically determined, excepting >300 keV electrons. Hence, we determine the first high-latitude point of electron flux enhancements as the low-latitude edge of ORB. Geographic latitude of this point is determined for each year with the accuracy varying from 0.5° to 1°. In Figure 3, one can find that the latitude of the ORB edge above Siberia decreases with years from ~65° to 60° for all energy range of electrons. The change of ORB location above the Europe and North America is not so obvious.

Figures 4 and Figure 5 show long-term variations in the location of ORB and corresponding predictions of the IGRF-12 model during 17 years from 2001 to 2018. As one can see, the ORB maximum and inner edge of >30 keV electrons are usually located at higher latitudes than those of >100 keV electrons, and the ORB of subrelativistic >300 keV electrons is located at lowest latitudes. Note that the location of ORB maximum for >30 keV electrons is scattered significantly and it is different from those for the more energetic electrons because of substantial contamination from the auroral electrons. In contrast, the ORB maxima and inner edge of >100 keV and >300 keV electrons demonstrate very similar dynamics.

As can be seen in Figures 4 and 5, the location of ORB manifests the well-known solar cycle variation: the latitudes of ORB maximum and inner edge have a tendency to be highest around solar minimum in 2008 – 2010 and lowest during solar maxima in the years 2001 and 2012 – 2013. However, during the declining phase of the current solar cycle (the years 2016 – 2018), the latitudes of ORB maximum and inner edge increased only slightly or even decreased above North America and especially above Siberia. Unfortunately, there is no any model of the ORB location variation with the solar cycle because the driving mechanisms are not well established.

As a first approach, the variations of ORB location with years are considered as random and can be fitted by a linear function (indicated by dashed strait lines in Figures 4 and 5):

$$\lambda = a * \text{year} + b, \quad (1)$$

where λ is the latitude of maximum or inner edge of ORB. The slope a, parameter b and their standard errors are calculated from a linear regression for various longitudinal regions and various energies of electrons. The results are presented in Tables 3 and 4 for the ORB maximum and the inner edge, respectively.

The linear fits are compared with geomagnetic field trends predicted by the IGRF model in different regions. The trends were calculated in the following manner. First, we took a point with given geographic coordinates and calculated its magnetic coordinates for the quiet day on 29 June 2001 using the IGRF model of epoch 2000. Namely, for the ORB maximum, we took points (70°N, 80°W), (66°N, 0°E) and (54°N, 100°E), respectively, for the American, European and Siberian sectors and calculated their geomagnetic coordinates (64.12°N, 11.44°W), (67.05°N, 95.66°E) and (59.5°N, 174.3°E), respectively. For the inner edge of ORB, we took, respectively, (46.5°N, 80°W), (59°N, 0°E) and (63°N, 100°E), with corresponding geomagnetic coordinates (56.62°N, 10.61°W) (60.59°N, 89.34°E) and (52.47°N, 173.7°E). Then we supposed that the geomagnetic coordinates of the points do not change with time and we used them to calculate geographic coordinates from the IGRF-12 model for corresponding quiet days listed in Table 2. The geographic coordinates of a point with given magnetic coordinates should be changed with time because of long-term variation of the geomagnetic field. As one can see in Figures 4 and 5, the long-term variation is almost linear function of the year and, hence, this variation can be easily compared with the linear fits of the ORB location.

In the American sector (see Figure 4a), the latitude of ORB maximum demonstrates a little decrease of about 1° while the IGRF-12 model predicts an increase of ~1°. The decrease results from relatively low latitudes, where the ORB maximum is located from 2013 to 2018. The location of inner edge of ORB in the American sector (see Figure 5a) does not practically change within the experimental uncertainty of ~1°. Note that in both cases, the slope *a* has very large error (see Tables 3 and 4). The errors are comparable or even exceed the values of slope. Hence, from the statistical consideration one can conclude that the model prediction does not contradict to the observations.

In the European sector (Figures 4b and 5b), the IGRF-12 model predicts very small change of 0.3° in the ORB location that is in good agreement with the ORB maximum dynamics. The location of ORB inner edge for electrons with energies >30 keV and >100 keV demonstrates an increase of ~3°. However, the slope of increase is determined with a substantial error of up to 50% (see Table 4) that produces an increase by only ~1.5°. In addition, the >300 keV electrons follow the model and do not exhibit any prominent trend. Hence in the European sector, the IGRF model predicts the ORB dynamics with sufficient accuracy.

in the Siberian sector, the IGRF model predicts ~1° decrease in latitude of the ORB maximum and inner edge as shown in Figures 4c and 5c. From the POES observations, we find that the ORB maximum is displaced to lower latitudes by at least ~3° in all electron energy channels: from ~69° to ~66° for >300 keV electrons, from ~70° to 66° for >100 keV electrons and from ~71° to 67° for >30 keV electrons (see Figure 4c). The difference is related to very low latitudes (~67° and less) of the ORB maximum during solar maximum and on the declining phase of the current 24th solar cycle in the years 2012 - 2013 and 2016 - 2018, respectively. In the solar maximum and on the declining phase of the previous 23rd solar cycle (the years 2001 and 2004 - 2006), the ORB maximum was located at higher latitudes (above 67°). Note that the error in determination of the slope *a* is ~50% as shown in Table 3. Hence statistically, the decrease of latitude might be two times smaller, i.e. ~1.5° to 2°. This decrease is slightly larger than 1° of the model prediction, within 0.5° to 1° statistical uncertainty in determination of latitude.

Similar pattern can be found for the inner edge of ORB in the Siberian sector (see Figure 5c). Namely, the IGRF model predicts a decrease of ~1°. The inner edge was shifted toward lower latitudes by ~3°, ~2° and ~1°, respectively, for >30 keV, >100 keV and >300 keV electrons. From Table 4, one can see that the slope *a* is calculated with errors of ~30% and ~20%, respectively, for >30 keV and >100 keV electrons. It means that the decrease in latitude might be ~2° (instead of ~3°) and ~1.5° (instead of ~2°), respectively. These values are again larger than 1° of the model prediction. Hence, there is a tendency that the change in the latitudinal location of ORB maximum is underestimated by the model. This fact indicates that during 17 years from 2001 to 2018, ORB is abnormally displaced toward the lower latitudes in the Siberian sector.

It is interesting to point out the year 2017, when the maximum and inner edge of ORB shifted to very low latitudes of 62° and ~59° respectively. The shift was observed during two quiet days on 9 and 10 June 2017. Similar pattern of displacement can be found on the declining phase of the previous 23rd solar cycle in the year 2005, when the ORB suddenly shifted equatorward by more than ~2°. Note that if we exclude the year 2017 from the linear fitting then the results are not practically changed because ORB is located at relatively low latitudes during the years 2012 to 2018.

4. Discussion

We have found up to 4° equatorward displacement of the ORB in the Siberian sector. The displacement is larger than that predicted by the IGRF-12 model. The difference is statistically significant. It might result both from a change of the geomagnetic field and from changes of driving parameters such as geomagnetic activity, the tilt angle, IMF *B*z and solar wind dynamic pressure. It is well known that those parameters affect the latitudinal location of domains in the outer magnetosphere (e.g. Kuznetsov et al., 1993; Newell et al., 2006). The effect of geomagnetic activity was eliminated by the choice of quiet days. The other drivers are considered below.

The tilt angle in the noon region at given longitude (80°W, 0°E and 100°E) varies a little (<2°) during the June month. The change of local time in 2-hour vicinity of noon produces ~5° variation of the tilt angle. The tilt angle variations of a few degrees result in a tiny change of ~0.1° in the ORB latitude (Newell et al., 2006; Dmitriev et al., 2010). Hence, we can neglect the effect of tilt angle.

The effect of solar wind parameters, including IMF *B*z and dynamic pressure (*P*d), to the outer magnetosphere domains was comprehensively investigated by Newell et al. (2006). Namely it was shown a dependence of the cusp low-latitude boundary on the IMF Bz such that *B*z = -4 nT results in less than 0.5° equatorward shift. The cusp location can be considered as a proxy of the ORB boundary. Similar situation can be found with the solar wind dynamic pressure: a change of *P*d from 1 to 2 nPa results in ~0.2° decrease in the latitude of the ORB boundary. Hence, the effects of both *P*d and IMF Bz are several times weaker than the difference of 3°.

Another possible effect is the solar cycle variation. It was well established that during solar maxima, the ORB is located at lower latitudes than during solar minimum. Variations of the ORB location from cycle to cycle are not investigated yet. We can only speculate that lower solar activity (solar minimum) results in an increase of the ORB latitudes. In Figure 3, one can see that the intensities of electrons are weaker after the beginning of the 24th solar maximum in 2012 in comparison with the 23rd solar cycle, which was stronger than the 24th one. Following this logic, the ORB should be located at relatively higher latitudes during the weak 24th solar cycle than during the strong 23rd solar cycle. However, we have found totally opposite effect: ORB over Siberia is located at lower latitudes after 2012.

From the above, we can conclude that the difference between the observations and predictions can be rather originated from anomalous dynamics of the geomagnetic field. This idea is supported by the observations of ORB location over the Europe and North America, where the ORB displacement is well predicted by the IGRF-12 model. An additional support can be found from results of long-term magnetic observations in Siberia where significant anomalies of the main geomagnetic field have been revealed in the 80°-130° longitudinal range (Gvishiani et al., 2014). Namely, the IGRF-12 model predicted the magnetic field up to 300 nT stronger than that measured by ground based magnetic stations that was close to 0.5% of the total magnetic filed in this region. For the geodipole, stronger magnetic field corresponds to higher latitudes.

In Figures 4c and 5c, one can see that the decrease of ORB latitude in the Siberian sector is most prominent after 2012. On the other hand in the years 2012 –2013, a sudden change was found in the acceleration of secular variation in the geomagnetic field (Finlay et al., 2015). Analyzing time interval from 1999 to 2015, Finlay et al. (2015) revealed 3 pulses in time evolution of the mean square secular acceleration power: in 2006, in 2009 and in 2012 – 2013. Chulliat et al. (2015) attribute these pulses, or so-called sharp geomagnetic "jerks", to magnetic field variations originating in the Earth’s core.

We can assume that the abnormal ORB displacement might be related to the geomagnetic jerk occurred in 2012 – 2013. The several degrees equatorward displacement of ORB in the Siberian sector indicates an equatorward shifting of all domains in the outer magnetosphere, including the region of auroral precipitations. Apparently, the shifting contributes to the increase in occurrence rate of the mid-latitude auroras in Siberia and, perhaps, in entire Russia. In addition, Finlay et al. (2015) expect that the next jerk might occur around 2016. We do not have any reports about the recent jerks yet. But very strong decrease of the ORB latitude observed in 2017 might indicate the sudden change in the geomagnetic field.

5. Conclusions

NOAA/POES observations of electrons with energies of few tens and hundreds of keV allowed revealing and measure a latitudinal displacement of the outer radiation belt during last 18 years. The displacement corresponds qualitatively to the change of geomagnetic field predicted by the IGRF-12 model. However in the Siberian sector, the model has a tendency to underestimate the equatorward shift of ORB. ~~However, numerically the equatorward shift in the Siberian sector was~~

~~found more than ~2° larger than that predicted by the model.~~ The shift became prominent after 2012 that might be related to the geomagnetic jerk occurred in 2012 – 2013. The increase in the occurrence rate of mid-latitude auroras in the Eastern Hemisphere can be explained, at least partially, by the equatorward displacement of the high-latitude projection of the outer magnetosphere domains.

Acknowledgments The authors thank a team of NOAA's Polar Orbiting Environmental Satellites for providing experimental data about energetic particles, the CDAWEB for providing the Wind solar wind data, and Kyoto World Data Center for Geomagnetism (http://wdc.kugi.kyotou.ac.jp/index.html) for providing the geomagnetic indices and computation of the IGRF12 model. The work was supported by grant MOST-106-2111-M-008-015-, R&D foundation from National Central University and partially by grant NSC103-2923-M-006-002-MY3/14-05-92002HHC_a of Taiwan - Russia Research Cooperation.

References

Asikainen, T., and Mursula, K.: Correcting the NOAA/MEPED energetic electron fluxes for detector efficiency and proton contamination, J. Geophys. Res. Space Physics, 118, doi:10.1002/jgra.50584, 2013.

Baker, D. N., Jaynes, A. N., Kanekal, S. G., Foster, J. C., Erickson, P. J., Fennell, J. F., Blake, J. B., Zhao, H., Li, X., Elkington, S. R., Henderson, M. G., Reeves, G. D., Spence, H. E., Kletzing, C. A., and Wygant, J. R.: Highly relativistic radiation belt electron acceleration, transport, and loss: Large solar storm events of March and June 2015, J. Geophys. Res. Space Physics, 121, 6647-6660, doi:10.1002/2016JA022502, 2016.

Case, N. A., MacDonald, E. A., and Patel, K. G.: Aurorasaurus and the St Patrick's Day storm, Astronomy & Geophysics 56(3), 13-14. DOI: 10.1093/astrogeo/atv089, 2015.

Chulliat, A., Hulot, G., and Newitt, L. R.: Magnetic flux expulsion from the core as a possible cause of the unusually large acceleration of the north magnetic pole during the 1990s, J. Geophys. Res., 115, B07101, doi:10.1029/2009JB007143, 2010.

Chulliat A., Alken, P., and Maus, S.: Fast equatorial waves propagating at the top of the Earth's core. Geophys Res Lett., 42(9), 3321-3329, doi:10.1002/2015GL064067, 2015.

Cresswell-Moorcock, K., Rodger, C. J., Kero, A., Collier, A. B., Clilverd, M. A., Häggström, I., and Pitkänen, T.: A reexamination of latitudinal limits of substorm-produced energetic electron precipitation, J. Geophys. Res. Space Physics, 118, 6694-6705, doi:10.1002/jgra.50598, 2013.

Dmitriev, A. V., Jayachandran, P. T., and Tsai, L.-C.: Elliptical model of cutoff boundaries for the solar energetic particles measured by POES satellites in December 2006, J. Geophys. Res., 115, A12244, doi:10.1029/2010JA015380, 2010.

Engebretson, M., Glassmeier, K.-H., Stellmacher, M., Hughes, W. J., and Luhr, H.: The dependence of high-latitude Pc5 wave power on solar wind velocity and on the phase of high-speed solar wind streams, J. Geophys. Res., 103, 26,271-26,283, doi:10.1029/97JA03143, 1998.

Evans, D. S., and Greer, M. S.: Polar Orbiting Environmental Satellite Space Environment Monitor: 2. Instrument Descriptions and Archive Data Documentation, Tech. Memo. Version 1.4, NOAA Space Environ. Lab., Boulder, Colo., 2004.

Finlay, C. C., Aubert, J., and Gillet, N.: Gyre-driven decay of the Earth's magnetic dipole, Nat. Commun, 7:10422, 1 - 8, doi: 10.1038/ncomms10422, 2016.

Gvishiani, A., Lukianova, R., Soloviev, A., Khokhlov, A.: Survey of Geomagnetic Observations Made in the Northern Sector of Russia and New Methods for Analysing Them, Surv. Geophys.,35, 1123-1154, DOI 10.1007/s10712-014-9297-8, 2014.

Horne, R. B., Thorne, R. M., Glauert, S. A., Meredith, N. P., Pokhotelov, D., and Santolik, O.: Electron acceleration in the Van Allen radiation belts by fast magnetosonic waves, Geophys. Res. Lett., 34, L17107, doi:10.1029/2007GL030267, 2007.

Kataoka, R., Shiota, D., Kilpua, E., and Keika, K.: Pileup accident hypothesis of magnetic storm on 17 March 2015, Geophys. Res. Lett., 42, 5155-5161, doi:10.1002/2015GL064816, 2015.

Kuznetsov, S.N., Suvorova, A.V., and Tolstaya, E.D.: Relationship of the cleft latitude to interplanetary parameters and DST variations, Cosmic Research, 31(4), 409-415 (Translated from Kosmicheskie Issledovaniya), 1993.

Lam, M. M., Horne, R. B., Meredith, N. P., Glauert, S. A., Moffat-Griffin, T., and Green, J. C.: Origin of energetic electron precipitation >30 keV into the atmosphere, J. Geophys. Res., 115, A00F08, doi:10.1029/2009JA014619, 2010.

Li, X., Baker, D. N., Kanekal, S. G., Looper, M., and Temerin, M.: Long term measurements of radiation belts by SAMPEX and their variations, Geophys. Res. Lett., 28(20), 3827-3830, DOI: 10.1029/2001GL013586, 2001.

MacDonald, E. A., Case, N. A., Clayton, J. H., Hall, M. K., Heavner, M., Lalone, N., Patel, K. G., and Tapia, A.: Aurorasaurus: A citizen science platform for viewing and reporting the aurora, Space Weather, 13, doi:10.1002/2015SW001214, 2015.

Mikhalev, A. V., Beletsky, A. B., Kostyleva, N. V., and Chernigovskaya, M. A.: Midlatitude Auroras in the South of Eastern Siberia during Strong Geomagnetic Storms on October 29-31, 2003 and November 20-21, 2003, Cosmic Research, 42(6), 591-596 (Translated from Kosmicheskie Issledovaniya, 42(6), 616-621), 2004.

Miyoshi, Y. and Kataoka, R.: Solar cycle variations of outer radiation belt and its relationship to solar wind structure dependences, Journal of Atmospheric and Solar-Terrestrial Physics, 73(10), 77-87, doi:10.1016/j.jastp.2010.09.031, 2011.

Miyoshi, Y. S., Jordanova, V. K., Morioka, A., and Evans, D. S.: Solar cycle variations of the electron radiation belts: Observations and radial diffusion simulation, Space Weather, 2, S10S02, doi:10.1029/2004SW000070, 2004.

Newell, P. T., Sotirelis, T., Liou, K., Meng, C.-I., and Rich, F. J.: Cusp latitude and the optimal solar wind coupling function, *J. Geophys. Res.*, 111, A09207, doi:10.1029/2006JA011731, 2006.

Newell, P. T., Sotirelis, T., and Wing, S.: Seasonal variations in diffuse, monoenergetic, and broadband aurora, *J. Geophys. Res.*, 115, A03216, doi:10.1029/2009JA014805, 2010.

Reeves, G. D., Spence, H. E., Henderson, M. G., Morley, S. K., Friedel, R. H. W., Funsten, H. O., Baker, D. N., Kanekal, S. G., Blake, J. B., Fennell, J. F., Claudepierre, S. G., Thorne, R. M., Turner, D. L., Kletzing, C. A., Kurth, W. S., Larsen, B. A., and Niehof, J. T.: Electron Acceleration in the Heart of the Van Allen Radiation Belts, Science, 341(6149), 991-994, DOI: 10.1126/science.1237743, 2013.

Roble, R. G., and Ridley, E. C.: An auroral model for the NCAR thermospheric general circulation model (TGCM), *Ann. Geophys.*, 5, 369-382, 1987.

Rodger, C. J., Clilverd, M. A., Green, J. C., and Lam, M. M.: Use of POES SEM-2 observations to examine radiation belt dynamics and energetic electron precipitation into the atmosphere, J. Geophys. Res., 115, A04202, doi:10.1029/2008JA014023, 2010.

Shen, X.-C., Hudson, M. K., Jaynes, A., Shi, Q., Tian, A., Claudepierre, S., Qin, M.-R., Zong, Q.-G., and Sun, W.-J.: Statistical study of the storm time radiation belt evolution during Van Allen Probes era: CME- versus CIR-driven storms, J. Geophys. Res. Space Physics, 122, 8327.8339, doi:10.1002/2017JA024100, 2017.

Shiokawa, K., Ogawa, T., and Kamide, Y.: Low-latitude auroras observed in Japan: 1999–2004, J. Geophys. Res., 110, A05202, doi:10.1029/2004JA010706, 2005.

Smith, A. R. A., Beggan, C. D., Macmillan, S., and Whaler, K. A.: Climatology of the auroral electrojets derived from the along-track gradient of magnetic field intensity measured by

POGO, Magsat, CHAMP, and Swarm. Space Weather, 15, https://doi.org/10.1002/2017SW001675, 2017.

Suvorova, A. V., Dmitriev, A. V., Tsai, L.-C., Kunitsyn, V. E., Andreeva, E. S., Nesterov, I. A., and Lazutin, L. L.: TEC evidence for near-equatorial energy deposition by 30 keV electrons in the topside ionosphere, J. Geophys. Res. Space Physics, 118, 4672-4695, doi:10.1002/jgra.50439, 2013.

Thebault E. et al.: International Geomagnetic Reference Field: the 12th generation, Earth, Planets and Space, 67:79, 2 – 19, doi 10.1186/s40623-015-0228-9, 2015.

Vázquez, M., Vaquero, J. M., Gallego, M. C., Roca Cortés, T., Pallé, P. L.: Long-Term Trends and Gleissberg Cycles in Aurora Borealis Records (1600 - 2015), Solar Phys 291, 613-642, DOI 10.1007/s11207-016-0849-6, 2016.

Table 1. Observations of discrete aurora in Russia in the years 2015 to 2016

Date	min Dst, nT	City	Geomagnetic location	Reference
2015 March 17-18	-220	Moscow	51°16N 122°06E	Ref1
2015 June 22-23	-200	Moscow	51°16N 122°06E	Ref2
2015 August 16-17	-84	St. Petersburg	56°23N 117°36E	Ref3
2015 October 7-8	-120	St. Petersburg	56°23N 117°36E	Ref4
2016 February 17-18	-50	St. Petersburg	56°24N 117°37E	Ref5
2016 April 3-4	-50	St. Petersburg	56°24N 117°37E	Ref6
2016 August 24-25	-80	St. Petersburg	56°24N 117°37E	Ref7
2017 September 7-8	-124	Novosibirsk	45°56N 160°07E	Ref8
2017 November 7-8	-74	St. Petersburg	56°25N 117°38E	Ref9

Ref1 - www.dp.ru/a/2015/03/18/Severnoe_sijanie_uvideli_zh/
Ref2 - www.dp.ru/a/2015/06/23/Severnoe_sijanie_uvideli_v/
Ref3 - http://47news.ru/articles/92419/
Ref4 - www.dp.ru/a/2015/10/08/Severnoe_sijanie_v_Peterbu/
Ref5 - www.fontanka.ru/2016/02/17/058/
Ref6 - www.dp.ru/a/2016/04/03/ZHiteli_Peterburga_deljatsja/
Ref7 - www.fontanka.ru/2016/08/24/035/ and www.topnews.ru/news_id_92986.html
Ref8 - http://www.ntv.ru/video/1515160/
Ref9 - https://www.fontanka.ru/2017/11/07/134/

Table 2. List of quiet days in June selected for POES observations of the outer radiation belt.

Year	Day in June	Start UT	Duration, hours	V* km/s	Pd** nPa	Bz_{min}[$] nT	POES Satellites[#]
2001	29	0	24	350	1.6 (1.0 – 3.2)	0.6 (-4)	P6
2002	28	0	24	340	1.2 (0.8 – 1.8)	2.2 (-3)	P6
2004	24	12	24	330	1.1 (0.5 – 2.5)	1.2 (-2)	P6, P7
2005	21	0	18	350	0.9 (0.5 – 2.0)	3.1 (-4)	P6, P7, P8
2006	23	0	24	310	1.6 (1.1 – 2.3)	3.4 (-1)	P6, P7, P8
2008	13	0	24	310	1.5 (0.8 – 1.9)	1.8 (-0.8)	P2, P7, P8
2009	17	0	24	300	1.1 (0.5 – 1.7)	1.9 (-3)	P2, P7, P8, P9
2010	12	0	24	350	1.1 (0.6 – 2.4)	0.2 (-2)	P2, P7, P8, P9
2011	28	6	24	390	0.8 (0.5 – 1.7)	1.8 (-2)	P2, P6, P8, P9
2012	15	0	24	320	0.8 (0.5 – 1.3)	0.0 (-3)	P2, P6, P8, P9
2013	16	0	24	330	0.9 (0.6 - 1.5)	1.0 (-3)	P2, P6, P8, P9
2014	1	0	36	300	1.7 (1.1 – 4.0)	1.5 (-4)	P1, P2, P9
2015	4	0	24	280	1.0 (0.7 – 1.7)	0.9 (-3)	P1, P2, P9
2016	3	0	24	300	1.0 (0.7 – 1.4)	-0.3 (-3)	P1, P2, P9
2017	9	6	24	310	1.9 (1.0 – 2.6)	-1.3 (-4)	P1, P2, P9
2018	12	8	24	300	1.3 (0.9 – 2.0)	0.0 (-4)	P1, P2, P9

*Daily average of the solar wind velocity

**Daily average of the solar wind dynamic pressure and its minimum and maximum in brackets

[$]Daily average Bz component of the interplanetary magnetic field and Bz minimum in brackets

#POES satellites observed the outer radiation belt

Table 3. Coefficients of the best linear fit of the latitudinal change of the ORB maximum location with years for various longitudes and energy of electrons

Longitude, deg	Energy, keV	a, deg/year	b, deg
-80	>30	-0.153 ± 0.112	362
-80	>100	-0.069 ± 0.097	192
-80	>300	-0.057 ± 0.084	167
0	>30	0.021 ± 0.089	24
0	>100	-0.032 ± 0.063	129
0	>300	-0.027 ± 0.042	119
100	>30	-0.265 ± 0.119	602
100	>100	-0.208 ± 0.106	486
100	>300	-0.167 ± 0.084	403

Table 4. Coefficients of the best linear fit of the latitudinal change of the ORB inner edge location with years for various longitudes and energy of electrons.

Longitude, deg	Energy, keV	*a*, deg/year	*b*, deg
-80	>30	-0.029 ± 0.065	106
-80	>100	-0.021 ± 0.059	89
-80	>300	-0.014 ± 0.063	73
0	>30	0.195 ± 0.107	-332
0	>100	0.241 ± 0.078	-424
0	>300	0.032 ± 0.069	-4
100	>30	-0.183 ± 0.058	432
100	>100	-0.211 ± 0.037	487
100	>300	-0.097 ± 0.069	257

Figure captions

Figure 1. Solar wind and geomagnetic conditions on 22 to 24 June 2006 (from top to bottom): solar wind bulk velocity V; solar wind dynamic pressure Pd; interplanetary magnetic field magnitude B (blue dotted curve) and Bz component (black solid curve); auroral electrojet index AE; storm-time *Dst* index. The day on 23 June (indicated by vertical red dashed lines) is very quite in the solar wind and geomagnetic parameters.

Figure 2. Geographic maps of energetic electron fluxes with energies >300 keV (a,b), >100 keV (c,d), >30 keV (e,f) and pitch angles of ~90° observed by POES satellites at height of ~850 km in 2 hour vicinity of local noon (left column) on 23 June 2006 and (right column) on 2 June 2016. The solid wide curve indicates the geomagnetic equator. The outer and inner electron belts and a slot region between them are clearly seen (excepting of >300 keV electrons), respectively, at high and middle latitudes in the longitudinal range from ~90° E to ~80°W.

Figure 3. Latitudinal profiles of electron fluxes with pitch angles of ~90° observed by POES satellites during quiet days in different years at height of ~850 km in vicinity of local noon at longitudes around 100°E (red circles), 0°E (blue crosses), and 80°W (black diamonds) for various energy channels: (a) >30 keV, (b) >100 keV, and (c) >300 keV. Vertical dashed and solid lines indicate latitudes of the maximum and inner edge of the outer radiation belt, respectively.

Figure 4. Geographic latitude of the maximum of the outer radiation belt measured at height of ~850 km during geomagnetic quiet days around 80°W (a), 0°E (b), and 100°E (c) for electrons with energies of >30 keV (red circles), >100 keV (blue crosses), and >300 keV (green triangles). Dashed curves of corresponding colors show the best linear fit of the latitudinal change of the maximum location with years (see Table 3). Solid black curves show the latitudinal change predicted by the IGRF model of corresponding epochs (see details in the text). The grey curve shows sunspot number (right axis).

Figure 5. The same as Figure 4 but for the inner edge of the outer radiation belt. Coefficients of the best linear fit are presented in Table 4.

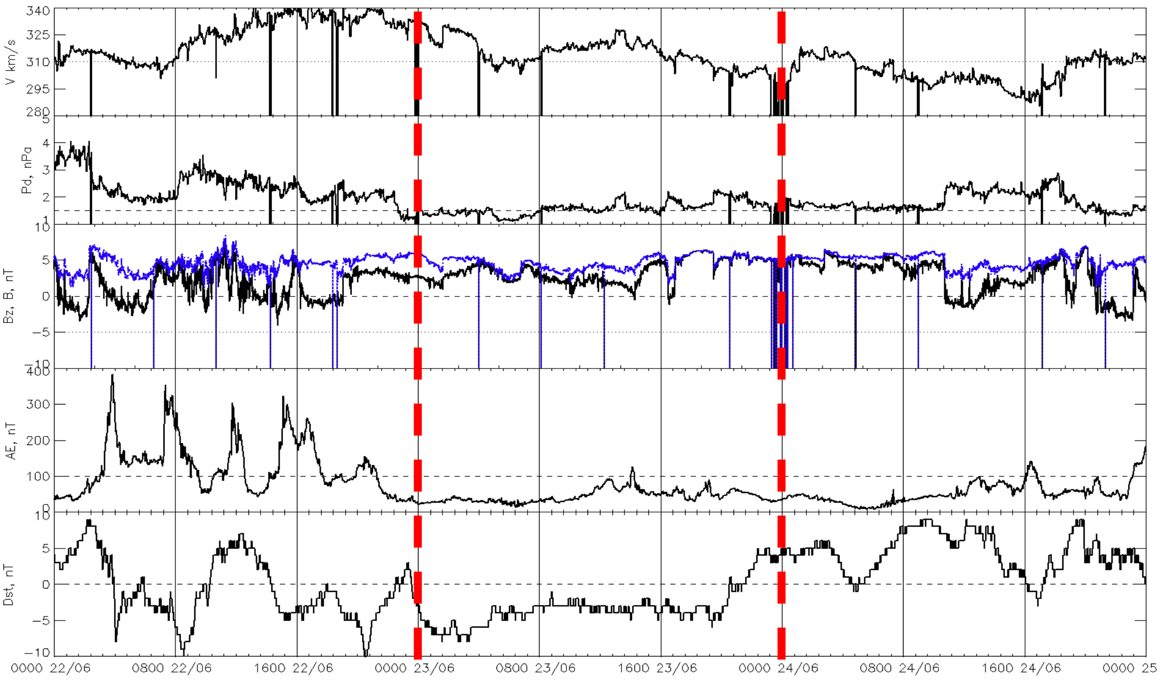

Figure 1. Solar wind and geomagnetic conditions on 22 to 24 June 2006 (from top to bottom): solar wind bulk velocity V; solar wind dynamic pressure Pd; interplanetary magnetic field magnitude B (blue dotted curve) and Bz component (black solid curve); auroral electrojet index AE; storm-time *Dst* index. The day on 23 June (indicated by vertical red dashed lines) is very quite in the solar wind and geomagnetic parameters.

2006

2016

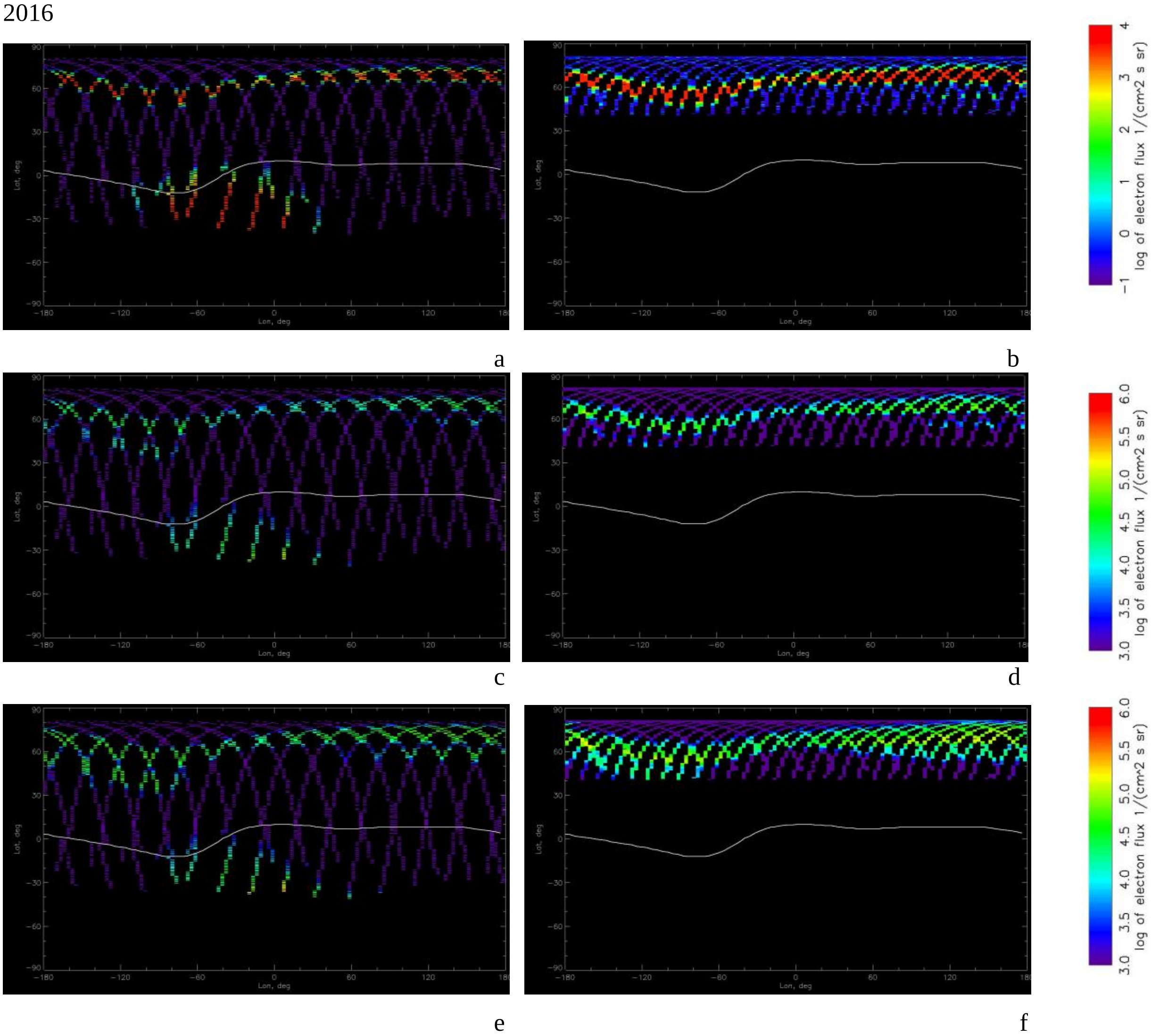

Figure 2. Geographic maps of energetic electron fluxes with energies >300 keV (a,b), >100 keV (c,d), >30 keV (e,f) and pitch angles of ~90° observed by POES satellites at height of ~850 km in 2 hour vicinity of local noon (left column) on 23 June 2006 and (right column) on 2 June 2016. The solid wide curve indicates the geomagnetic equator. The outer and inner electron belts and a slot region between them are clearly seen (excepting of >100 keV electrons), respectively, at high and middle latitudes in the longitudinal range from ~90° E to ~80°W.

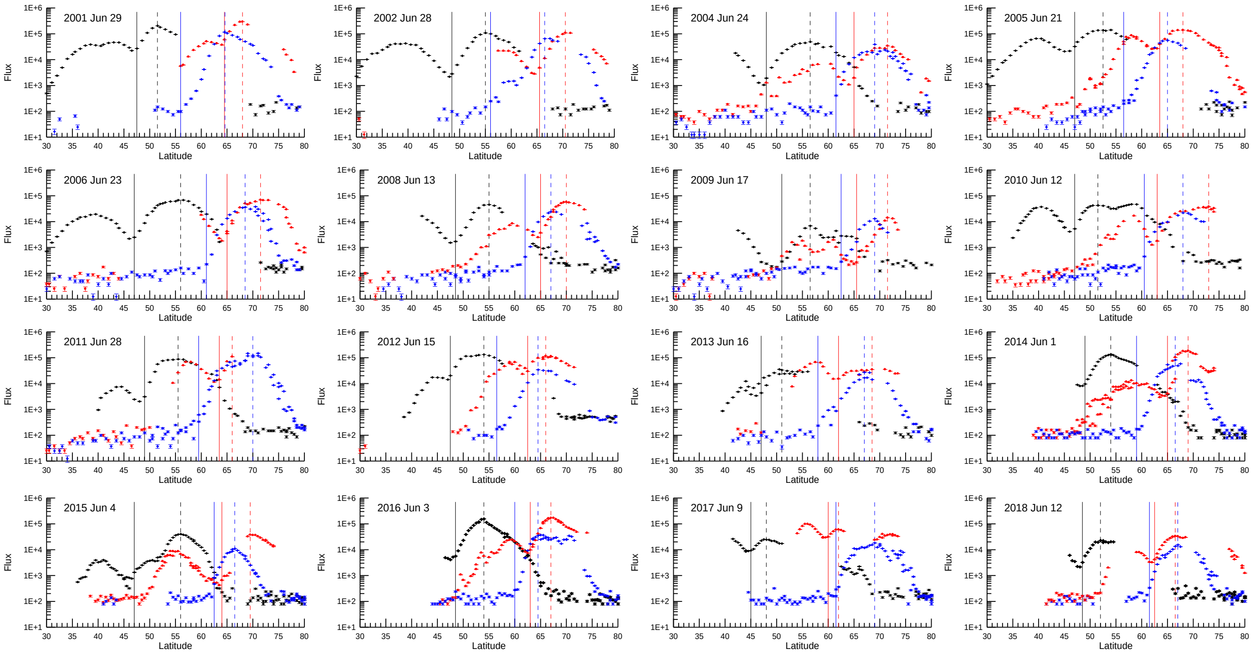
2001 Jun 29
2002 Jun 28
2004 Jun 24
2005 Jun 21
2006 Jun 23
2008 Jun 13
2009 Jun 17
2010 Jun 12
2011 Jun 28
2012 Jun 15
2013 Jun 16
2014 Jun 1
2015 Jun 4
2016 Jun 3
2017 Jun 9
2018 Jun 12
Flux
Latitude

a

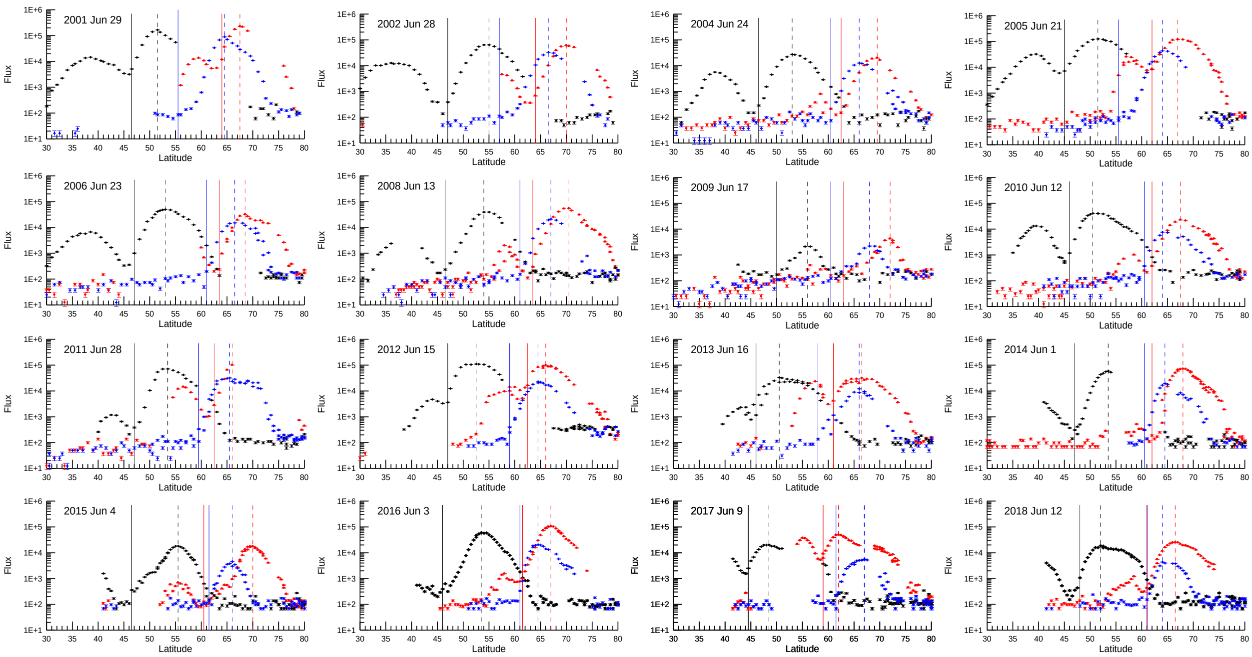
2001 Jun 29
2002 Jun 28
2004 Jun 24
2005 Jun 21
2006 Jun 23
2008 Jun 13
2009 Jun 17
2010 Jun 12
2011 Jun 28
2012 Jun 15
2013 Jun 16
2014 Jun 1
2015 Jun 4
2016 Jun 3
2017 Jun 9
2018 Jun 12
Flux
Latitude

b

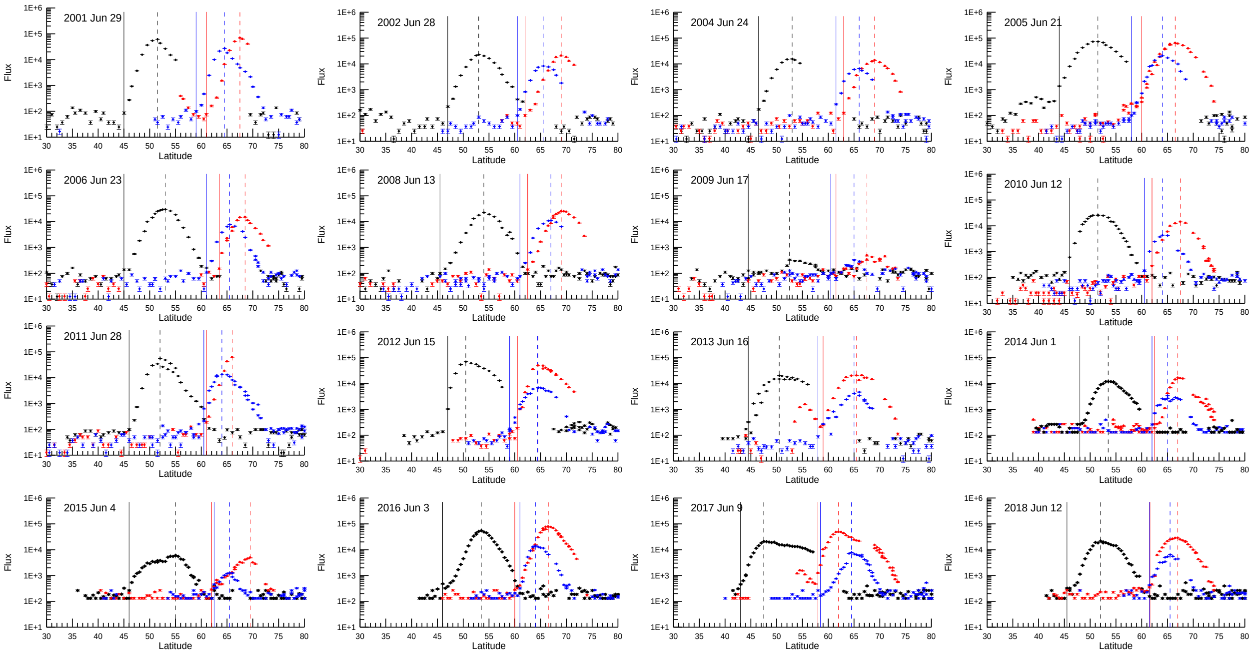

c

Figure 3. Latitudinal profiles of electron fluxes with pitch angles of ~90° observed by POES satellites during quiet days in different years at height of ~850 km in vicinity of local noon at longitudes around 100°E (red circles), 0°E (blue crosses), and 80°W (black diamonds) for various energy channels: (a) >30 keV, (b) >100 keV, and (c) >300 keV. Vertical dashed and solid lines indicate latitudes of the maximum and inner edge of the outer radiation belt, respectively.

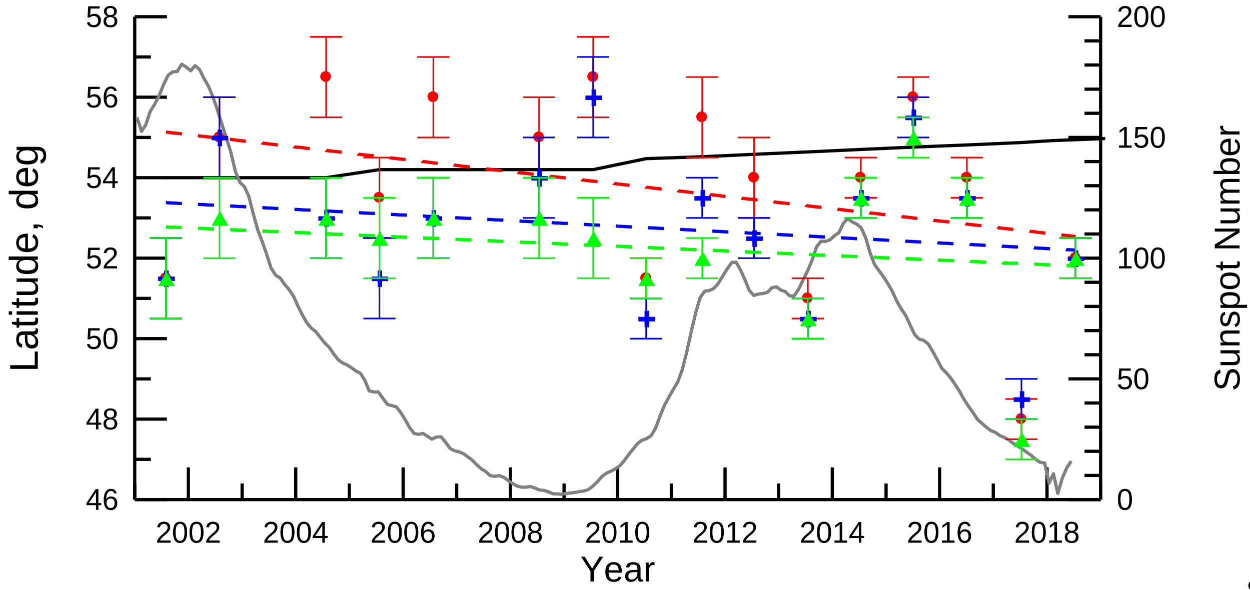

Latitude, deg
Sunspot Number
Year
58
56
54
52
50
48
46
200
150
100
50
0
2002
2004
2006
2008
2010
2012
2014
2016
2018

a

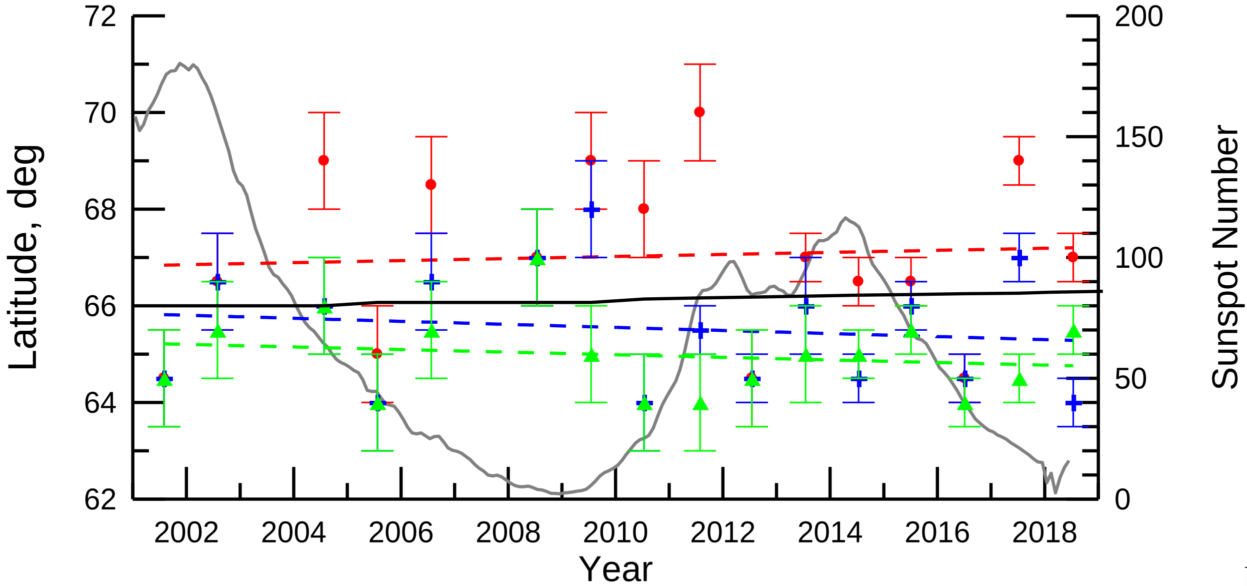

Latitude, deg
Sunspot Number
Year
72
70
68
66
64
62
200
150
100
50
0
2002
2004
2006
2008
2010
2012
2014
2016
2018

b

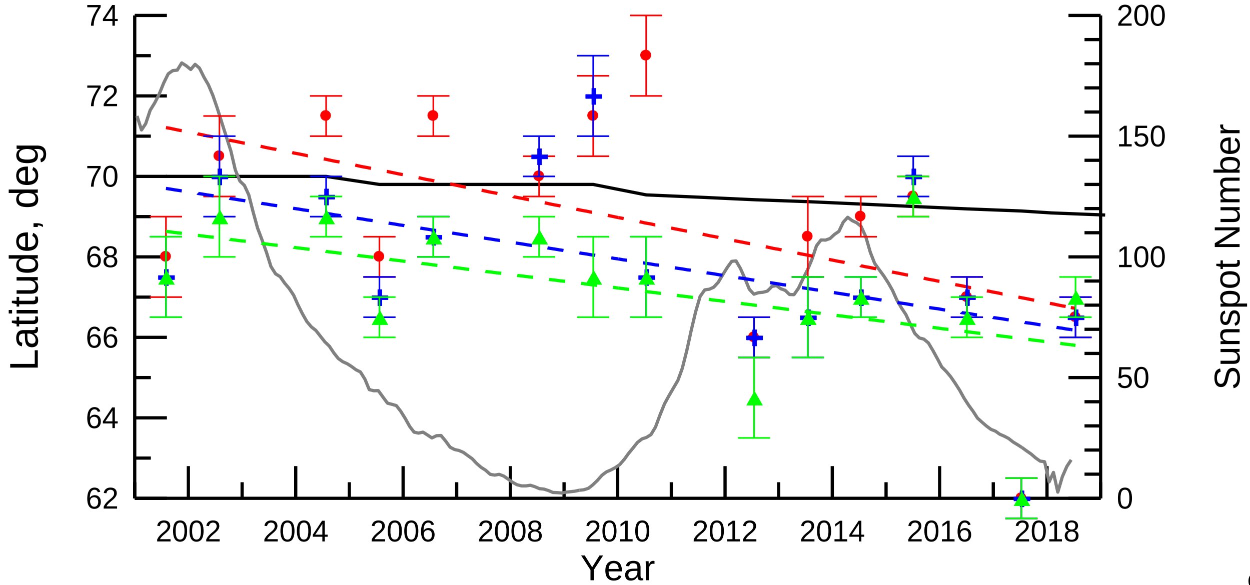

Latitude, deg
Sunspot Number
Year
74
72
70
68
66
64
62
200
150
100
50
0
2002
2004
2006
2008
2010
2012
2014
2016
2018

c

Figure 4. Geographic latitude of the maximum of the outer radiation belt measured at height of ~850 km during geomagnetic quiet days around 80°W (a), 0°E (b), and 100°E (c) for electrons with energies of >30 keV (red circles), >100 keV (blue crosses), and >300 keV (green triangles). Dashed curves of corresponding colors show the best linear fit of the latitudinal change of the maximum location with years (see Table 3). Solid black curves show the latitudinal change predicted by the IGRF model of corresponding epochs (see details in the text). The grey curve shows sunspot number (right axis).

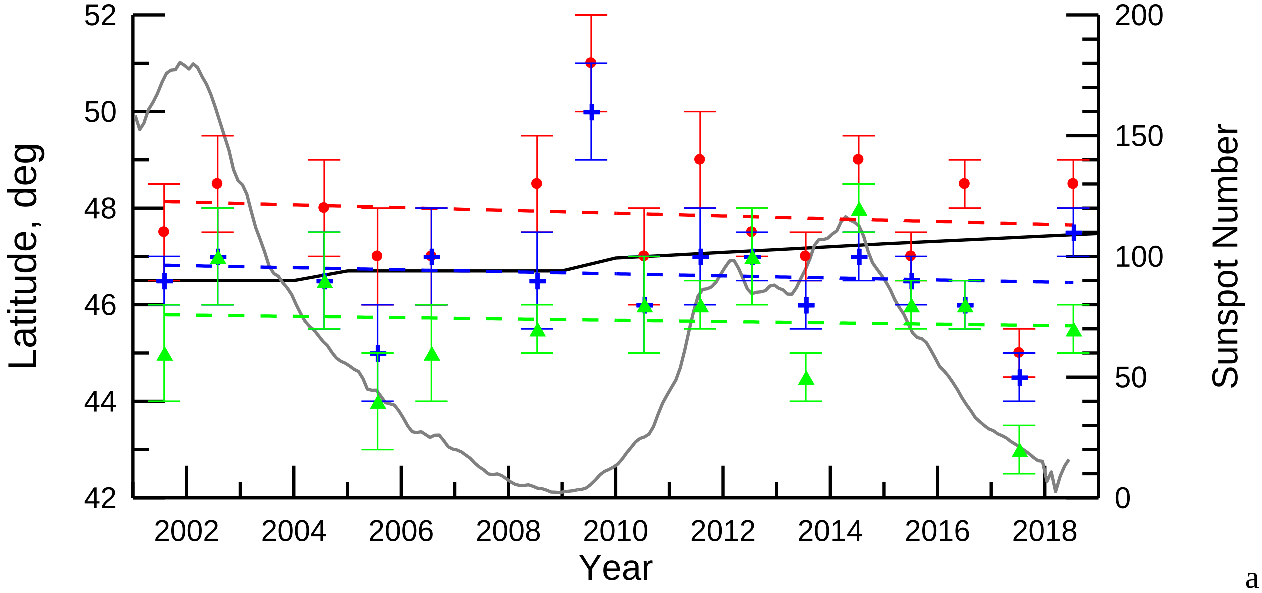
52
50
48
46
44
42
200
150
100
50
0
2002
2004
2006
2008
2010
2012
2014
2016
2018
Year
Latitude, deg
Sunspot Number

a

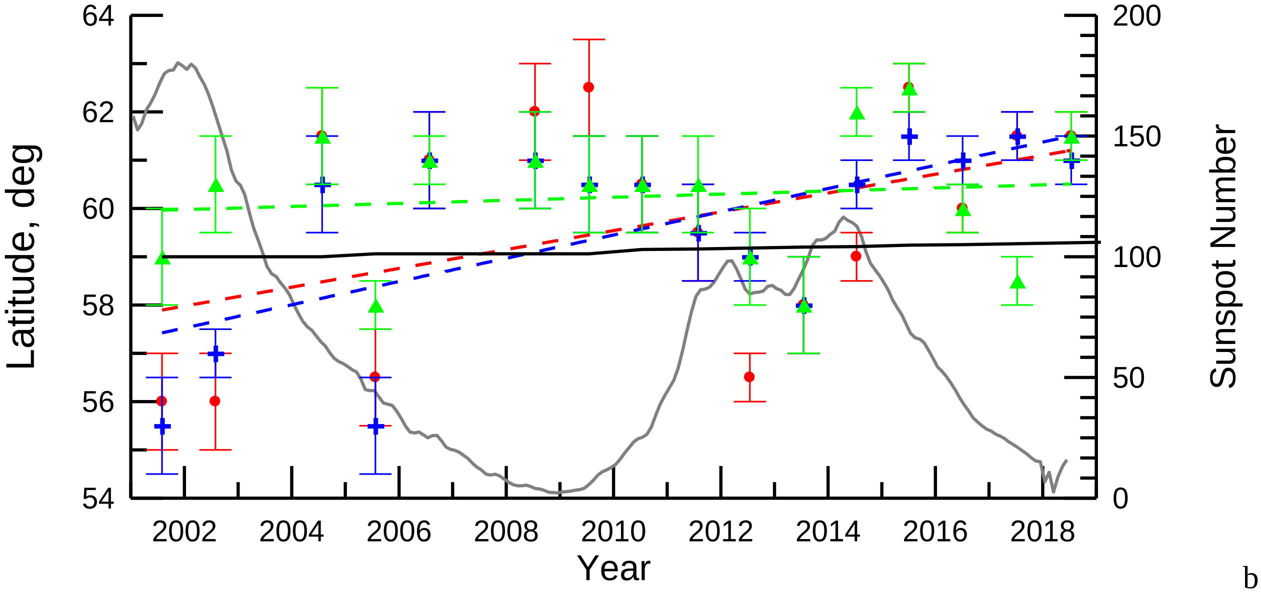
64
62
60
58
56
54
200
150
100
50
0
2002
2004
2006
2008
2010
2012
2014
2016
2018
Year
Latitude, deg
Sunspot Number

b

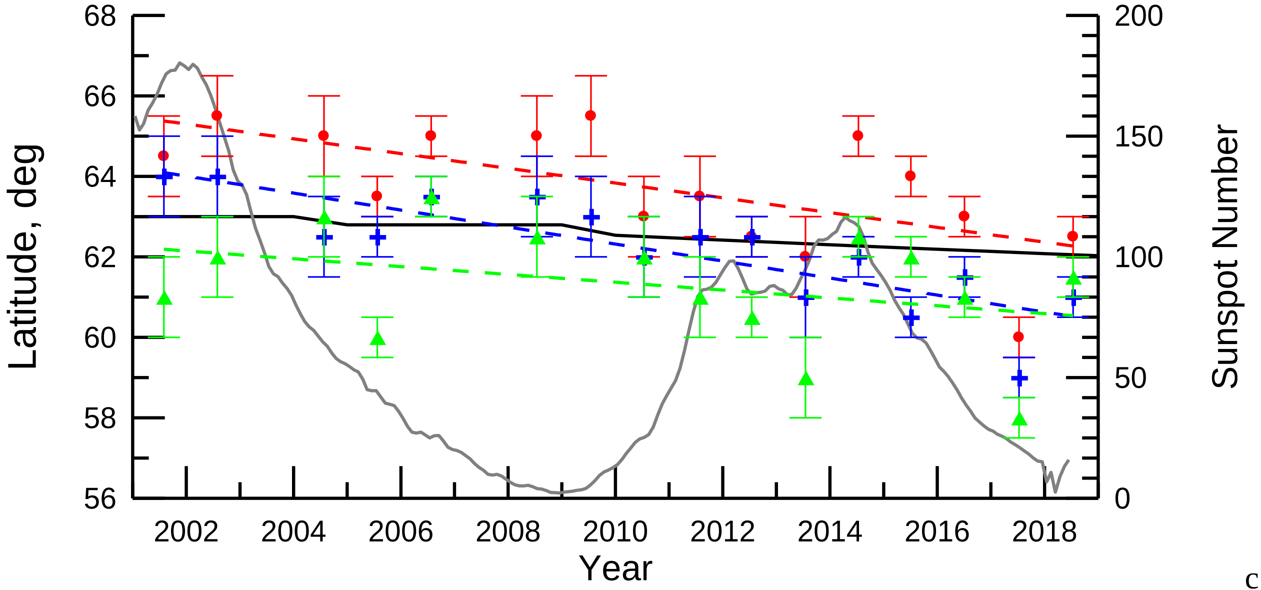
68
66
64
62
60
58
56
200
150
100
50
0
2002
2004
2006
2008
2010
2012
2014
2016
2018
Year
Latitude, deg
Sunspot Number

c

Figure 5. The same as Figure 4 but for the inner edge of the outer radiation belt. Coefficients of the best linear fit are presented in Table 4.